Ultrafast reproducible synthesis of a Ag-nanocluster@MOF composite and its superior visible-photocatalytic activity in batch and in continuous flow

ARTICLE

Ultrafast reproducible synthesis of an Agnanocluster@MOF composite and its superior visible-photocatalytic activity in batch and in continuous flow

Received 00th January 20xx,
Accepted 00th January 20xx

DOI: 10.1039/x0xx00000x

Ana Arenas-Vivo,[a] Sara Rojas,[a] Iván Ocaña,[a] Ana Torres,[a] Marta Liras,[b,*] Fabrice Salles,[c] Daniel Arenas-Esteban,[d] Sara Bals,[d] David Ávila,[e] Patricia Horcajada[a,*]

The (photo)catalytical properties of Metal-Organic Frameworks (MOFs) can be enhanced by postsynthetic inclusion of metallic species in their porosity. Due to their extraordinarily high surface area and well defined porous structure, MOFs can be used for the stabilization of metal nanoparticles with adjustable size within their porosity. Originally, we present here an optimized ultrafast photoreduction protocol for the *in situ* synthesis of tiny and monodispersed silver nanoclusters (AgNCs) homogeneously supported on the photoactive porous titanium carboxylate MIL-125-NH_2 MOF. The strong metal-framework interaction between -NH_2 and Ag atoms influences the AgNCs growth, leading to the surfactant free efficient catalyst AgNC@MIL-125-NH_2 with improved visible light absorption. The potential use of AgNC@MIL-125-NH_2 was further tested in challenging applications: *i)* the photodegradation of the emerging organic contaminants (EOCs) methylene blue (MB-dye) and sulfamethazine (SMT-antibiotic) in water treatment, and *ii)* the catalytic hydrogenation of *p*-nitroaniline (4-NA) to *p*-phenylenediamine (PPD) with industrial interest. It is noteworthy that compared with the pristine MIL-125-NH_2, the composite presents an improved catalytic activity and stability, being able to photodegrade 92% of MB in 60 min, 96% of SMT in 30 min, and transform 100% of 4-NA to PPD in 30 min. Aside from these very good results, this study describes for the first time the use of a MOF in a visible light continuous flow reactor for wastewater treatment. With only 10 mg of AgNC@MIL-125-NH_2, a high SMT removal efficiency over 70% is maintained after >2 h using water flow conditions found in real wastewater treatment plants, envisioning a future real application of MOFs in water remediation.

Introduction

In the last years, water pollution is becoming a major concern due to novel and dangerous anthropogenic pollutants.[1] Particularly, emerging organic contaminants (EOCs) are found as hundreds contaminating water resources and include a wide different array of compounds: pharmaceuticals and personal care products (PPCPs), dyes, pesticides, veterinary products, industrial products, and engineered nanomaterials.[2] EOCs enter the environment from a large variety of sources and pathways (*e.g.,* wastewater treatment plants (WWTPs), hospital effluents, livestock activities, and industrial waste),[3] leading to concentrations in surface waters (even in tap drinking water) capable of causing detrimental effects to living organisms (from $ng{\cdot}L^{-1}$ to $\mu g{\cdot}L^{-1}$).[4,5] It is therefore clear that currently used technologies are not equipped to remove them and more effective methods need to be developed.

Among the new processes to eliminate EOCs from water (*i.e.,* ozonization,[6] chlorination,[7] sonodegradation,[8] biodegradation,[9] catalysis,[10] activated carbon treatment[11]), photocatalysis shows great potential since it could be performed by sunlight illumination at ambient conditions. Metal oxide and chalcogenides semiconductors (*e.g.*, TiO_2, ZnO, Fe_2O_3, CdS, GaP, ZnS) are promising heterogeneous photocatalysts, but their large scale applications are limited due to difficult post-separation and low energy conversion efficiency.[12]

Metal-organic frameworks (MOFs), or crystalline porous coordination polymers,[13] outstand among other proposed materials for environmental remediation by photocatalysis, as they can act as both selective adsorbents of contaminants and catalysts, playing an active role in their degradation. They present many properties that commend them particularly in water treatment: *i)* large porosity (up to Brunauer–Emmett–Teller surface area (S_{BET}) = 7800 $m^2{\cdot}g^{-1}$),[14,15] associated with high sorption capacities; *ii)* active sites, where contaminants can be chemisorbed and/or degraded; *iii)* some are highly stable in water; *iv)* easily functionalizable cavities,

[a] *Advanced Porous Materials Unit, IMDEA Energy. Av. Ramón de la Sagra 3, 28935 Móstoles-Madrid, Spain.*
[b] *Photoactivated Process Unit, IMDEA Energy. Av. Ramón de la Sagra 3, 28935 Móstoles-Madrid, Spain.*
[c] *ICGM, Univ. Montpellier, CNRS, ENSCM, Montpellier, France.*
[d] *EMAT and NANOlab Center of Excellence, Univ. of Antwerp, Groenenborgerlaan 171, Antwerp 2020, Belgium.*
[e] *Department of Inorganic Chemistry, Chemical Sciences Faculty, Complutense University of Madrid, 28040 Madrid, Spain.*
* patricia.horcajada@imdea.org; marta.liras@imdea.org
Electronic Supplementary Information (ESI) available: Details of experimental procedures, characterization (XRPD, N_2 sorption, ATG, FTIR, ICP, TEM, HAADF-STEM, Tomography reconstruction, EDX, and DR), HPLC conditions, photocatalytic degradation and catalytic hydrogenation experiments, and simulation studies. See DOI: 10.1039/x0xx00000x

where specific host-guest interactions may take place; *v)* opportunities for tailoring the MOF structure to allow shape selective adsorption and/or catalysis; *vi)* MOFs could be synthesized at large scale (few already commercialized);[16] and *vii)* they can be shaped into practical devices adapted for decontamination (*e.g.,* pellets, membranes, columns).[17] MOFs have already proven remarkable performances on the removal (adsorption and/or catalytic degradation) of EOCs from water. However, the majority of these studies concerns organic dyes (70% of the reports) being PPCPs elimination an emerging topic, only studied from end-2012 (bibliographic estimation by WOS February 2021).[18] Which is more, studies presented up to date are limited to only batch type reactors and investigation of MOFs photocatalysts under continuous flow is still a remaining subject of analysis.[19,20]

Despite the advantages of MOFs for the catalytic degradation of EOCs, as indicated above, the type of active sites on MOFs is mainly limited to unsaturated metal centers, the creation of structural defects around metals, or active sites grafted on the organic linker. However, MOFs can also incorporate catalytically active guest species into their pore spaces. Integration of MOFs and noble metal ions or nanoparticles (NPs) (*e.g.,* Pt, Pd, Ag, Au) to form new multifunctional composites has become a rapidly developed research area. Their incorporation can result in an enhancement on the photoconversion quantum yield and allows the extension of the absorption band gap to visible light, enabling water remediation with sunlight.[21,22] The growing number of research articles on this topic indicates that NPs@MOF nanocomposites will play an important role in heterogeneous photocatalysis.[23] Particularly in water decontamination, some outstanding results have been reported in the use of MIL-100(Fe)@TiO_2 in the methylene blue (MB) degradation, reaching 45 times highest rate of MB degradation compared to TiO_2;[24] or MIL-125-NH_2@Ag/AgCl in the degradation of rhodamine B, with an 80% of degradation in only 10 min.[25]

Among other metallic nanospecies of great interest are silver nanoclusters (AgNCs) due to their unique electronic properties,[26] as they present high catalytic efficiency and fluorescence resonance energy transfer;[27] [28]tiny size (up to few nanometers);[29] low toxicity (*e.g.,* at 250 µM, cell viability is *ca.* 98% in human neonatal foreskin fibroblast cells),[30,31] and they are considered a less expensive alternative to AgNPs. Few reports have analyzed the use of MOFs as scaffolds for the growth and stabilization of AgNCs without the need of surfactants. However, long chemical reduction procedures with several steps have been followed, as in the complex infiltration procedures in the synthesis of Ag clusters (AgCs) within MIL-68, HKUST-1, MIL-101 or MOF-5,[32–35] ruling out their potential in real applications, like water remediation. Even UV photoreduction was previously used in the synthesis of Ag/rGO/MIL-125 composite, it required 2 h of irradiation to produce large AgNPs (5-15 nm) that were adsorbed on both, the reduced graphene oxide layers and the MOF outer surface.[36]

The work presented here describes an optimized ultrafast photoreduction protocol innovatively used for the formation of small AgNCs supported in the porosity of the photoactive Ti-MOF MIL-125-NH_2. MIL-125-NH_2 or $[Ti_8O_8(OH)_4(BDC\text{-}NH_2)_6]$ is built from Ti-oxo-clusters coordinated to the 2-aminoterephthalate ligand (BDC-NH_2). MIL-125-NH_2 has been selected as scaffold for the synthesis of AgNCs considering different factors: *i)* it represents a prototype and extensively studied carboxylate MOF family, *ii)* in terms of cost, it can be considered affordable in a future (already commercialized by different companies),[37,38] *iii)* its large surface area and high pore volume (S_{BET} ~1500 $m^2 \cdot g^{-1}$, V_p ~0.65 $cm^3 \cdot g^{-1}$ with octahedral ~12.5 Å and tetrahedral cavities ~6 Å, accessible via windows ~5–7 Å),[39] *iv)* the available amino groups, which may facilitate a strong metal-framework interaction between -NH_2 and Ag clusters, as previously reported for other MIL-125-NH_2 composites,[40,41] preventing AgNCs leaching and leading to the surfactant free efficient composite (AgNC@MIL-125-NH_2), and *v)* its theoretical band gap energy (E_g) of 2.6 eV, that enables semiconducting application under visible light, compatible with the degradation of EOCs using sunlight.[42] Aside from this innovative synthetic method, this study describes one of the earliest uses of a MOF in a visible light continuous flow reactor for wastewater treatment, and particularly the first working in a continuous linear flow without recirculating flow[43–46] If initially, we have considered the vis-photodegradation of the standard dye methylene blue for comparison reasons (MB + MOF+ water; February WOS ~ 600 papers, see chemical structure in **Figure 1**), later the photodegradation of a challenging antibiotic (sulfamethazine; SMT, **Figure 1**) was originally studied using a continuous flow homemade photoreactor. SMT presents a wide occurrence and relatively high level in natural aquatic environment (from 0.12 to 19.2 ppm),[3,47,48] associated with severe environmental and health issues (human average daily intake <0.05 ppm for preventing hormone unbalance, oral rat median lethal dose (LD_{50}) = 2 $g \cdot Kg^{-1}$).[49]

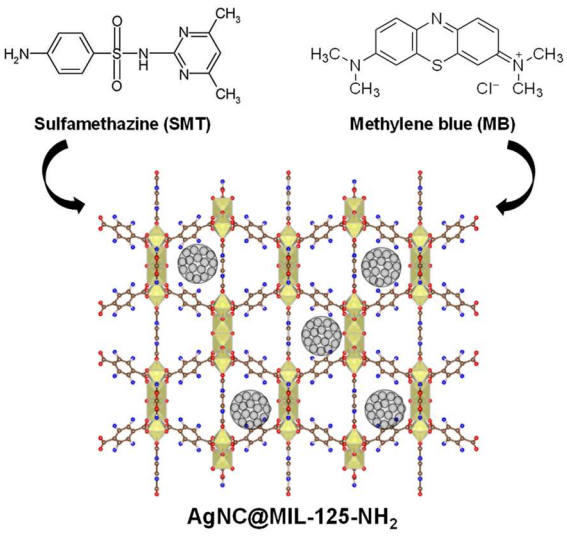

Figure 1. Schematic view of the structure of AgNP@MIL-125-NH_2, where the NH_2 groups have been represented in all the possible locations (titanium polyhedra, oxygen, nitrogen, and carbon are represented in yellow, red, blue, and brown, respectively; hydrogen atoms are omitted for clarity). Ag-NCs

are represented by grey spheres. Structure of the dye MB and antibiotic SMT are also given.

In all described studies, the EOCs photodegradation efficiency of the AgNC@MIL-125-NH_2 was compared with the pristine MIL-125-NH_2 and other reported photocatalysts, resulting in both, an improved activity and stability. Finally, due to the interest of AgNCs stabilization for other organic catalytic reactions, the AgNC@MIL-125-NH_2 was tested in the catalytic hydrogenation of *p*-nitroaniline (4-NA) to *p*-phenylenediamine (PPD), an important intermediate for a variety of industrial chemicals, resulting in very high efficiencies.[5051]

Results and discussion

Synthesis and characterization of AgNC@MIL-125-NH_2

The synthesis of stable AgNCs of controlled size supported on MOFs porosity by means of photo-induced transformation was pioneeringly pursued. This photoreduction protocol might enhance overall composite (photo)catalytic activity while overcoming the long and intricate silver chemical reduction. Our inspiration come from Maretti *et al.,*[52] and Garcia-Bosch *et al.,*[53] works where fluorescent AgNCs were photosynthesized by means of Irgacure as photoiniciator, and stabilized by the presence of cyclohexylamine and a polymer with pendant -NH_2 groups, respectively. In our case, the visible-light-sensitive MIL-125-NH_2 was selected as the ideal scaffold as bearing -NH_2 functional groups potentially able to stabilize the AgNCs, aside from its porosity which could enable size precise control during the photoreduction reaction.

Briefly, AgNCs@MIL-125-NH_2 was prepared by an easy and fast two-step procedure (for details see **Supporting Information (SI) section 3**). First, the silver precursor ($AgCF_3COO$) was impregnated within the MOF porosity prior diffusion (15 min). Then, the adsorbed silver was subsequently photoreduced in the presence of a photo-initiator (Irgacure-2959 or I-2959) in a controlled ultrafast way under stirring (15 s). To avoid the two main issues reported from bibliography (*i.e.,* preferential formation of AgNCs on the outer MOF surface, and polydispersity and heterogeneous distribution of AgNCs),[54] the design of the best synthetic strategy was optimized considering several parameters (irradiation time, reagents addition, stirring, MOF:Ag ratio; see transmission electron microscopy (TEM) images; **SI, section 3**). Discussing in brief their influence: *i) irradiation time*: excessive reaction time (15 s *vs*. 20 min or 1 h) leads to AgNCs aggregation through defect generation in the framework, procuring AgNPs larger than the pore size, even coming out after 1 h of irradiation (**SI**, **Figure S5**); *ii) reagent addition*: a stepwise procedure (impregnation, then irradiation) leads to a better distribution of the AgNC through the MOF crystals than one-pot impregnation/irradiation as well as better control of particle size(**SI, Figure S6**); *iii) stirring* during the photoreduction step not only improve the sample homogeneity, associated with homogeneously distributed and monodispersed AgNCs, but also allows faster reaction kinetics (15 s *vs*. 1 min in presence and absence of stirring; **SI, Figure S7**); and *iv) MOF:Ag ratio*: enables the modulation of the amount of stabilized Ag and directly affects to reaction yield (see **SI, Figures S8** and **Table S1**). In the end, a simple and efficient (yield >80% in only 20 min total process) two-step method was originally set up for obtaining tiny and monodispersed AgNCs (1.01 ± 0.36 nm, corresponding to ~28 Ag atoms; **SI, Figure S9**) homogeneously distributed within the microporosity of MIL-125-NH_2 (**Figure 2**). Electron tomography studies were performed in order to ensure the location of the AgNC within the MOF particles. Based on a careful segmentation through the slices of the reconstruction (**Figure 2e and f, SI**, **Figure S10** and **Movie 1**), the presence of the AgNCs within the MOF porous structure is confirmed. Moreover, many of the particles were found following same direction of the pores, thus supporting the porous structure during tilt series acquisition. Therefore, the synthetic procedure here presented ensured the formation of AgNC inside MIL-125-NH_2, overcoming the limitations of previous works with MOFs with AgNPs exclusively adsorbed on their outer surface.[32–36] The ultrafast photoreduction reaction (15 s) prevented AgNCs uncontrolled growing and aggregation, further confined by MOF porosity (as AgNCs growth was limited within the size of MIL-125-NH_2 cavities of *ca.* 0.61 and 1.25 nm).[39] The synthetic procedure was followed with the non-functionalized MIL-125 material, obtaining bigger Ag NPs (*ca.* 7 nm), mainly located on the outer surface of the MOF particles (**SI, Figure S11**). These results support the effect of the -NH_2 group in the stabilization of the AgNCs, withing the framework. To the best of our knowledge, this is the first time tiny AgNCs have been synthesized by photoreduction using MOFs as support, and outstands from other UV assisted silver photoreduction methods previously reported by means of reaction time, particle size and distribution within the porosity.[36] Further, images showed that the impregnation & photoreduction process was successful and barely aggressive with the MIL-125-NH_2 structure, which preserved its characteristic oval shape, with a relatively roughen surface. As the available -NH_2 seems to be the key, this ultrafast stabilization might be extrapolated to other photoactive microporous MOFs with available amino groups, such as the zirconium based UiO-66-NH_2.

Further characterization by inductively coupled plasma-optical emission spectrometry (ICP-OES) evidenced that a significant amount of Ag was incorporated into the porous matrix (7.5 ± 0.4 wt.%), as also confirmed by thermogravimetric analyses (TGA; 7.7 wt.%, **SI, Figure S12**) and semi-quantitative energy dispersive X-ray spectroscopy (EDX; Ti:Ag molar ratio = 7.0 ± 0.5 : 3.0 ± 0.5, or 21:1). Finally, the UV-vis solid reflectance spectroscopy revealed a significant change in AgNC@MIL-125-NH_2 light absorption, as reflectance increases beyond ~430 nm compared to the pristine MIL-125-NH_2 (**SI, Figure S13**). This is associated with a reduction of the direct allowed transition energy band gap, being 2.40 and 2.53 eV for AgNC@MIL-125-NH_2 and MIL-125-NH_2, respectively, due to the overlapping of the AgNC plasmon resonance band at ~450 nm (values obtained by the Tauc Plot).[55] This last result suggests a strong association between the AgNCs and MIL-125-NH_2, which might modify the photon absorption of the resulting composite.

The structural integrity of MIL-125-NH_2 after the AgNCs incorporation process was confirmed using X-ray powder diffraction (XRPD), with a slight decrease in crystallinity due to AgNCs accomodation (**SI, Figure S14**). In addition, the main reflections of the face-centered cubic (fcc) structure of Ag^0 could not be seen, supporting the small size of the AgNCs. XRPD patterns further confirmed the formation of pure AgNC@MIL-125-NH_2 as no characteristic reflections of $AgCF_3COO$ neither the photoiniciator I-2959 are observed. Fourier transform infrared spectroscopy (FTIR) also corroborated that the structure remains stable after the impregnation & photoreduction process, and the proper removal of I-2959 (peaks at 1700, 1200, 1100 cm^{-1}, **SI, Figure S15 and S16**). The AgNC@MIL-125-NH_2 composite preserves the main vibrational modes of the hosting MOF such as coordination of carboxylates to the titanium (1550 - 1450 cm^{-1}).

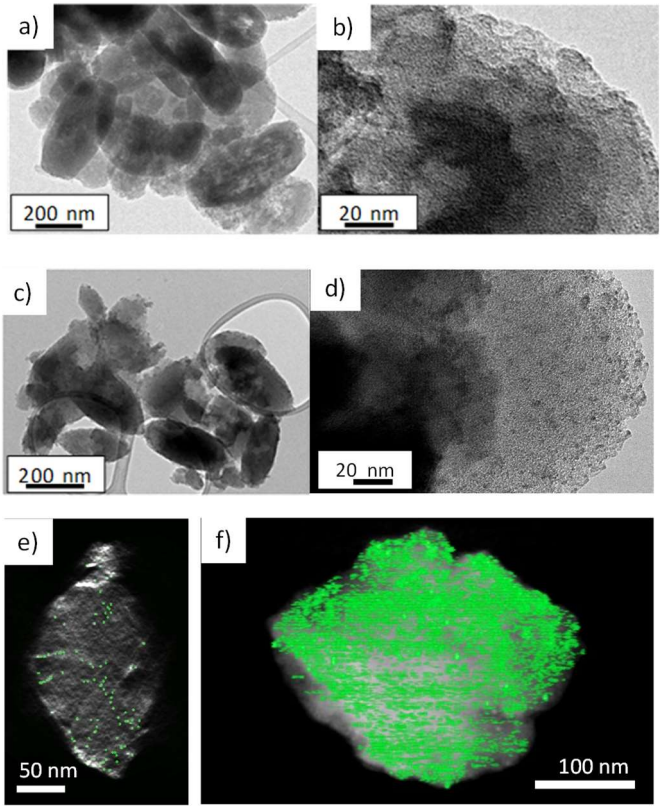

Figure 2. TEM micrographs of the pristine MIL-125-NH_2 (a, b), and the AgNC@MIL-125-NH_2 composite (c, d). Orthoslice of the HAADF tomography reconstruction of one particle from the AgNC@MIL-125-NH_2 composite (e), and the 3D reconstruction where the AgNCs have been carefully segmented in green (f). Scale bar: (a, c) 200 nm, (b, d) 20 nm, (e) 50 nm, and (f) 100 nm.

Furthermore, a red shift in the bands associated to the symmetric and asymmetric -NH_2 stretching (from 3459 and 3356 cm^{-1} in the pristine MOF, to 3442 and 3344 cm^{-1} in the AgNC@MIL-125-NH_2) suggests the stabilization of the AgNCs in the framework, and their interaction with the –NH_2 groups of the BDC-NH_2 ligand. This result is in agreement with previous FTIR modification, observed in the encapsulation of bigger AgNPs into the MIL-125-NH_2 solid.[40] This observation is also corroborated by the snapshots obtained from Monte Carlo simulations where AgNCs are distributed in the entire MOF porosity and the main interactions between Ag and MIL-125-NH_2 framework are observed with both the -NH_2 and benzene groups of the MIL-125-NH_2 (calculated distances = 2.8-2.9 Å, see **SI, Figure S27a**). Indeed, these large distances are mainly due to the absence of electrostatic interactions and only van der Waals interactions are taken into account in these calculations. The simulation results will be discussed in detail in the next section. Finally, the textural properties of both AgNC@MIL-125-NH_2 and the pristine MOF were evaluated by means of N_2 sorption at 77 K (**SI, Figure S17**). The specific surface area and pore volume of the composite were slightly lower than the pristine MOF (S_{BET} ~1430 *vs.* 1560 $m^2 \cdot g^{-1}$; V_p ~0.61 *vs.* 0.65 $cm^3 \cdot g^{-1}$, respectively), in agreement with the presence of AgNC in the composite. Hence the presence of the AgNCs within the cavities of MIL-125-NH_2 may explain these differences. Moreover, molecular simulation of AgNCs insertion gave reasonably similar textural properties for the composite (S_{BET} ~1390 *vs.* 1925 $m^2 \cdot g^{-1}$; V_p ~0.63 *vs.* 0.81 $cm^3 \cdot g^{-1}$, for AgNC@MIL-125-NH_2 and MIL-125-NH_2, respectively). Differences between experimental and calculated textural properties of pristine MIL-125-NH2 might be explained by the absence of defects and perfect porosity evacuation when simulating the crystalline structure of MIL-125-NH2. In addition, the difference between the experimental and simulated surface variation (ΔS = 130 and 535 m2·g-1, respectively) could be associated to the creation of some defects upon the AgNC loading/formation that counterbalance the occupancy of the voids.

Photodegradation of water emerging pollutants

To evaluate the ability of AgNC@MIL-125-NH_2 in water purification, the powdered material was first suspended in a tap water solution of the selected contaminant, using a concentration range within that one commonly found in wastewater (200 ppm of MB and 10 ppm of SMT).[48,56] AgNC@MIL-125-NH_2 photocatalytic activity towards the degradation of EOCs was investigated under visible light irradiation, quantifying the contaminant elimination. In addition, AgNC@MIL-125-NH_2 stability was monitored during the EOCs photodegradation process (**SI, Section 4**).

Methylene blue (MB)

Remarkably, AgNC@MIL-125-NH_2 was able to photodegrade up to 72 ± 4 and 92 ± 3% of MB present in the solution within only 10 and 60 min, respectively (**Figure 3**, red triangles). The pristine MIL-125-NH_2 displays a slower kinetics, reaching 48 ± 1 and 72 ± 2% of MB photodegradation in 10 and 60 min, respectively (**Figure 3**, dark red squares). The rapid MB elimination kinetics is most likely attributed to: *i)* the lower energy band gap induced by the AgNC plasmon resonance (2.40 *vs.* 2.53 eV in AgNC@MIL-125-NH_2 and MIL-125-NH_2, respectively); *ii)* the reduction of the electron hole recombination as AgNC work as electron trapping aggent;[57] and *iii)* the chemical affinity of Ag to the -S and -N atoms of MB structure.[58] This chemical affinity of

MB towards the AgNC@MIL-125-NH_2 is also seen in the experiments carried out in dark (**SI, Figure S18**), where MB physisorption trends are presented. After 60 min in dark, AgNC@MIL-125-NH_2 adsorpbed 70% of the dye while the pristine MOF only removed 40% of the MB from water (comparatively, the same photodegraded amount in 10 min, **Figure 3**). This interaction between the dye and the catalyst framework likely affects to its photodegradation under visible light.

To shed some light on the MB degradation kinetics and to gain further understanding on the involved mechanism, the MB degradation kinetics using AgNC@MIL-125-NH_2 and MIL-125-NH_2 were fitted to a second order kinetics according to Eqn. (1) (**SI, Section 4a**), giving rise to *k* values of 0.0007 and 0.0001 $g \cdot mg^{-1} \cdot min^{-1}$, respectively. It can be seen that AgNC@MIL-125-NH_2 is a better photocatalyst as its kinetic constant is 7 times higher than the pristine MOF (**SI, Figure S19**).

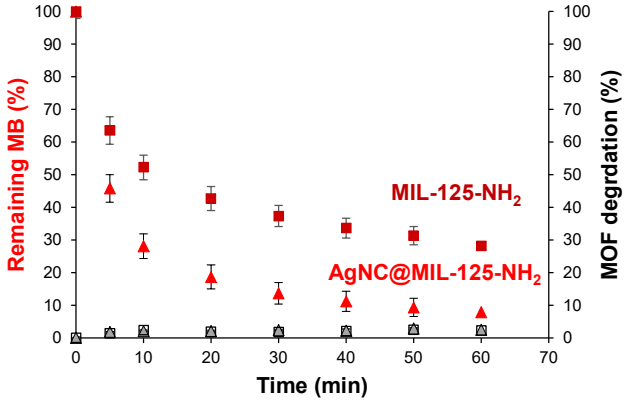

Figure 3. MB photodegradation kinetics under visible light irradiation in the presence of AgNC@MIL-125-NH_2 (red triangles, left y axis) and MIL-125-NH_2 (dark red squares, left y axis). The MOFs degradation by means of BDC-NH_2 leaching was also represented for AgNC@MIL-125-NH_2 (white squares, right y axis), and MIL-125-NH_2 (grey triangles, right y axis).

These fittings also reveal that the rate-limiting step of the photodegradation is not the physisorption of the dye on the MOF porous surface, but the photocatalytic reaction on the AgNCs active site, after MOF photon absorption by the ligand-to-cluster transfer mechanism.[59,60]

Further, both solids showed an excellent stability since only ~2% of the total BDC-NH_2 ligand was leached after 1 h contact (as determined by high-performance liquid chromatography-HPLC). This is in agreement with previous studies of MIL-125-NH_2 stability in water, as the BDC-NH_2 leached after 1 h is equivalent to the 5 $mg \cdot L^{-1}$ formerly reported, stating that visible light does not have a strong influence on MIL-125-NH_2 stability in water.[61] Besides, XRPD of both materials suggest the retainment of the crystalline character of the parenteral MIL-125-NH_2, with a slight peak broadening associated with the MB adsorption (**SI, Figure S20**). The crystalline structure of AgNC@MIL-125-NH_2 was not almost disturbed after photodegradation of MB, suggesting the stabilization of the MIL-125-NH_2 scafold by a potential "template" effect of the encapsulated AgNCs on its structure, reinforcing the composite. Note also here that upon TEM observations, we have observed a MIL-125-NH_2 stabilization effect under the beam by the presence of AgNCs. This increment in stability was also reported in the Pt@UiO-66-NH_2 composite after photocatalytic H_2 production.[62] These stability analyses are fundamental in water remediation. Despite, other MB photodegradation studies using MOFs do not often report these relevant data (**SI, Table S2**).

To deeply analyze the influence of AgNCs, the catalytic performances of AgNC@MIL-125-NH_2 were compared with its analogue AgNPs@MIL-125-NH_2, based on an equivalent amount of AgNPs with a larger size (5 *vs*. 1 nm), recently reported by our group (see experimental detail in the **SI, Section S4**).[40] Although AgNPs@MIL-125-NH_2 also provided a fast MB degradation at short times (84 ± 4% after 1 h; **SI Figure S21**), the kinetics is slightly faster when using AgNC@MIL-125-NH_2. TOF calculation (min^{-1}) also revealed this faint increment in activity (**SI, Figure S22**) evidencing the relevance of the higher reactive surface area of the AgNCs *vs*. AgNPs (~1.25 times higher surface area with AgNCs) and the size dependent response of the AgNC surface plasmon resonance for the photocatalytic reaction, since both materials possess the same Ag content. Previous bibliography considers this beneficial catalytic effect as a consequence of the variation of the proportion of accessible active sites.[63] The number of atoms on the surface and in the edges differs with catalyst shape and size, and the number of low coordinated atoms increases when the catalyst size decreases, incrementing the reaction rate. We can tentatively estimate that almost all the 28 atoms of the AgNCs are on the surface (against the *ca.* 25% for the AgNPs).[64] However, there are some limitations about determining the particle size effects in catalysis, since the catalyst' structure (shape) and even the MOF' structure (crystallinity, density of defects), and the different accommodation and distribution of the catalyst on the host MOF support may be changed during the synthesis. Our results here agree with diverse studies using AgNPs as heterogeneous catalyst in the hydrogenation of nitroaromatics or CO oxidation, in which the catalyst activity increased with the decrease in Ag size.[65,66] Finally, to further contextualize these results, AgNC@MIL-125-NH_2 showed a MB photodegradation capacity much higher than the widely-known commercial TiO_2, catalytically limited under visible light (18 ± 1%, 1 h, SI, **Figure S21**). Furthermore, the MB photodegradation capacity of AgNC@MIL-125-NH_2 is on the range, or even surpasses, the MB degradation capacity of other known MOFs and MOF composites (90% degradation in 60 min, **SI, Table S2**). Therefore, this work paves the way of the use of AgNC@MIL-125-NH_2 for the elimination of dyes as EOCs in wastewater due to its high photoactivity and aqueous stability.

Sulfamethazine (SMT)

The excellent MB removal capacity and stability of AgNC@MIL-125-NH_2 prompted us to further investigate the elimination of a challenging EOC, the antibiotic SMT, under more real continuous flow conditions. First, we studied the kinetics of the SMT photodegradation process under static conditions, reaching *ca.* 96.6 ± 0.2% of SMT removal in only 30 min (**SI,**

Figure S23) while keeping intact its crystalline structure and chemical integrity (**SI, Figures S23** and **S24**; 5 ± 2% degradation). The integrity of AgNCs was also confirmed by EDX analysis (Ti:Ag molar ratio before and after catalysis = 7.0 ± 0.5 : 3.0 ± 0.5 *vs.* 7.0 ± 0.1 : 2.6 ± 0.2, respectively). As previously obtained in MB degradation, the pristine MIL-125-NH_2 displays a slower kinetics than its AgNC counterpart, with almost half of the SMT degradation. Again, the SMT photodegradation data were fitted to a second order kinetics according to Eqn. (1) (**SI, Section 4b**), giving rise to *k* values of 3.56 and 0.02 $g \cdot mg^{-1} \cdot min^{-1}$ for AgNC@MIL-125-NH_2 and MIL-125-NH_2, respectively.

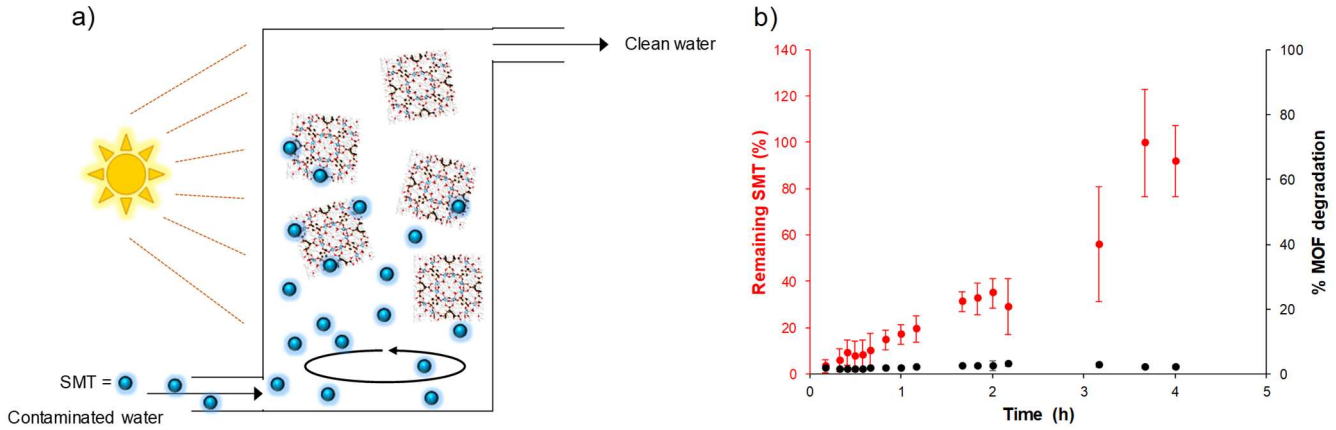

Figure 4. a) Schematic view of the AgNC@MIL-125-NH_2 based continuous flow system. b) Effect of time on the remaining SMT (red circles, left y axis) using AgNC@MIL-125-NH_2 reactor at a continuous flow of 30 $mL \cdot h^{-1}$ of a 10 ppm SMT solution in water. The potential leaching of the ligand (black triangles, right x axis) was also monitored. All studies were carried out in triplicate.

AgNC@MIL-125-NH_2 exhibits a *ca.* 200 times faster photodegradation kinetics than the pristine MOF (**SI, Figure S25**), being even faster than the three MOF-based materials reporting SMT degradation (**SI, Table S3**). Taking advantage of the efficient performance of AgNC@MIL-125-NH_2 in SMT photodegradation, for the first time a continuous linear flow photoreactor (without recirculation) was developed as proof-of concept of the use of MOF-based materials for the continuous efficient pollutant removal from water (**Figure 4a; SI, Section 4b**). Practically, a cylindrical glass photoreactor was designed and filled with AgNC@MIL-125-NH_2, pumping a continuous flow of SMT-contaminated tap water. As shown in **Figure 4b**, a high removal efficiency over 71 ± 12% was maintained after more than 2 h when using only 10 mg of catalyst under a flux of 30 $mL \cdot h^{-1}$ or 80 $L \cdot m^{-2} \cdot h^{-1}$, time after which is deactivated. It has to be pointed that the water flow applied during these experiments is within the range of the flow rate used in wastewater treatment plants (*i.e.,* 27 – 530000 $L \cdot m^{-2} \cdot h^{-1}$),[67] supporting the interest of AgNC@MIL-125-NH_2 as efficient photocatalyst in the practical removal of SMT. This flow is also comparable to other pure MOF-based systems, proposed for the EOCs removal by exclusively adsorption (100 $\mu L \cdot min^{-1}$ equivalent to 0.034 $mL \cdot m^{-2} \cdot h^{-1}$ for KOH@Ni_8BDP_6,[20] 0.05 $mL \cdot min^{-1}$ equivalent to 58 $L \cdot m^{-2} \cdot h^{-1}$ for ZIF-8,[68] and 2 $mL \cdot min^{-1}$ equivalent to 764 $L \cdot m^{-2} \cdot h^{-1}$ for MIL-101(Cr)).[69] However, the flow rate can be significantly increased when using different substrates as MOFs support (0.45 $L \cdot h^{-1}$ for PES-SPES/MIL-53(Al)-NH_2/PTFE without indicating the membrane surface,[70] 6.45 $L \cdot m^{-2} \cdot h^{-1}$ for LacPAN-MIL-101-L,[71] 125.7 $L \cdot m^{-2} \cdot h^{-1} \cdot bar^{-1}$ for UiO-66-NH_2@MMM,[72] and 1000 $L \cdot m^{-2} \cdot h^{-1}$ for UiO-66@wood).[73] This implies that our system, able to remarkably treat 6.50 $L \cdot h^{-1} \cdot g^{-1}$ of contaminated water *via* visible light photocatalytic degradation, could be further improved by supporting the MOF on a specific substrate. After the continuous flow experiment, the chemical integrity of AgNC@MIL-125-NH_2 was confirmed (1.9 ± 0.5% of ligand leaching after 4 h; **Figure 4b**). However, there is a loss of crystallinity which may be the reason of the deactivation of the photocatalyst. There is a significant broadening of the Bragg peaks (**SI, Figure S26**), consistent with a loss of crystallinity, which may hamper the access of the SMT to the porosity of the MOF, where the AgNCs are located.

In order to understand the impact of the presence of AgNCs in the MIL-125-NH_2 porosity on the adsorption of pollutants, Monte Carlo simulations were performed for pristine MIL-125-NH_2 and AgNC@MIL-125-NH_2 for the adsorption of SMT at low coverage (1 or 2 molecules *per* unit cell, **SI, Figure S27 and S28**). From these calculations, it was possible to extract the main adsorption sites and compare the behavior of the EOC guest hosted within the porosity. In the pristine MIL-125-NH_2, SMT molecules strongly interacted with the MOF (theoretical adsorption enthalpy close to 127 $kJ.mol^{-1}$). The main adsorption sites are evidenced by the extracted configurations from Monte Carlo: -NH_2 from SMT can interact by hydrogen bonds with the amino groups of the MIL-125-NH_2 (N_{SMT}---H_{MOF} = 2.652 Å; H_{SMT}---N_{MOF} = 2.54 Å), while secondary adsorption sites can also be observed between -NH_2 or -SO_2 groups from SMT and the carboxylate groups from the MOF (H_{SMT}---$O_{carbMOF}$ = 2.964 Å; O_{SMT}---$C_{carbMOF}$ =2.885Å) (**SI, Figure S27b**).

Regarding the AgNC@MIL-125-NH_2, it could be seen that the SMT guest molecules were found in the large octahedral cavities (~12.5 Å) together with AgNCs (**SI, Figure S27c**). Furthermore, the main interaction sites are again associated to the formation of hydrogen bonds between the amino groups from the SMT and the MOF (with larger H_{SMT}---N_{MOF} distances ranging between 2.6 and 2.7 Å; as a typical illustration on **SI, Figure S27d**, we observe a 2.682 Å distance). In addition, AgNCs

interact with the benzene rings of the SMT (distances 2.7-3.0 Å). FTIR spectra of both SMT-loaded materials (MIL-125-NH_2_SMT and AgNC@MIL-125-NH_2_SMT**, SI, Figure S29**) confirm the configurations found by molecular simulation. A shift in the characteristic stretching ν_{asym}(N-H) and ν_{sym}(N-H) vibration bands of the amino group of the MOF (from 3360 to 3376 cm^{-1} for the AgNC@MIL-125-NH_2; and from 3349 and 3446 cm^{-1} to 3386 and 3497 cm^{-1} for the MIL-125-NH_2) suggests the formation of interactions between these moieties. Finally, in the case of the pristine MIL-125-NH_2, there is a shift of around 20 cm^{-1} in the bands associated to the carboxylate groups found in the range of 1520-1650 cm^{-1} and 1280 to 1400 cm^{-1} for the ν_{asym} and ν_{sym}, respectively. This shift is not visible in the AgNC@MIL-125-NH_2_SMT solid, in total agreement with the simulation observations.

As a final point, a successful design of a water remediation continuous flow system requires prediction of the concentration-time profile or breakthrough curve for the effluent. Here, the efficiency of the system was assessed by the curve shape and the breakthrough time. The so-called Thomas model is commonly used in the modeling of fixed bed breakthrough curves in environmental sorption research (see **SI, Section 4** for further details).[74] From this equation, values describing the characteristic operational parameters of the column can be determined from a plot of *Ct*/*Co* against *t* at a given bed height and flow rate using the non-linear regressive method. Thus, the Thomas model was found suitable for the description of whole breakthrough curve, with good correlation values (R^2 = 0.9624; **SI, Figure S30**). This model, considering Langmuir kinetics of the degradation process and no axial dispersion, is derived with the assumption that the rate driving force abbeys second-order reversible reaction kinetics,[75] giving a quite good kinetic constant (K_{Th}) of 3.49 mL $mg^{-1}\cdot min^{-1}$. However, a direct comparison with other MOF-continuous flow systems is impossible since all the studies reported so far are exclusively based on sorption processes (mainly vapor phase) and not catalytic ones. In an attempt to position our results within the context of EOCs elimination from water, a comparison can be made with the kinetic constants obtained using MOFs or other adsorbent materials (*i.e.,* the adsorption of diazinon using MIL-100(Cr): K_{Th} = 5.11 – 8.33 $mL\cdot min^{-1}\cdot mg^{-1}$, breakthrough time from 0 to 13 min,[69] sulfamethazole with lignite activated coke: K_{Th} = 0.04 - 0.01 $mL\cdot mg^{-1}\cdot min^{-1}$,breakthough time from 0 to 2 h, [76] or atenolol with activated carbon: K_{Th} = 2.28 $mL\cdot mg^{-1}\cdot min^{-1}$, breakthrough time from 0 to 124 h).[77] Finally, although this laboratory scale MOF photoreactor is still far from its application in wastewater treatments, our work presents one of the few examples of continuous-flow photodegradation of EOCs using MOFs with a considerably good breakthrough time and working under operation conditions on the range of those normally applied in wastewater treatment plants.

On the whole, the efficient removal of SMT and MB contaminants by AgNC@MIL-125-NH_2 together with its water robustness under real water continuous flow and vis-irradiation, make this composite a highly promising photocatalyst for the removal of emerging contaminants in water.

Catalytic hydrogenation of 4-nitroaniline

AgNCs stabilization is not only of interest for the photodegradation of EOCs, but also for the catalysis of organic reactions at industrial scale. AgNPs have been previously reported for the hydrogenation of several nitroaromatic compounds.[78,79] In particular, *p*-nitroaniline (4-NA) is an important compound used as intermediate or precursor in the manufacture of organic synthesis, and it is used as target-model molecule in oxidation processes. In this context, heterogeneous catalysis using AgNCs supported on MOFs might be an interesting alternative for such processes, in terms of activity, lifetime and recyclability. In order to compare with other already described heterogeneous catalysts, the activity of AgNC@MIL-125-NH_2 towards catalytic hydrogenation of 4-NA to *p*-phenylenediamine (PPD) in the presence of $NaBH_4$ was studied, demonstrating its potential for further catalytic-related applications (**SI, Section 5**). As it can be seen from the **Figure 5**, complete hydrogenation of 4-NA is achieved at room temperature within 30 minutes when catalyzed by AgNC@MIL-125-NH_2. AgNCs are the active catalytic sites, as the pristine MIL-125-NH_2 barely produces *ca.* 4% of the maximum theoretical PPD while consuming *ca.* 20% of 4-NA leading to the formation of undesired secondary products (which identification is out of the scope of this work).

Analysis of the reaction kinetics enabled the determination of the rate constant with a satisfactory fitting to a first order reaction kinetics following the Eqn (3) (**SI, Section 5**). The fitting of the data gave rise to a *k* value of 0.119 and 0.002 min^{-1} for AgNC@MIL-125-NH_2 and MIL-125-NH_2, respectively (see **SI, Figure S33**). Results indicate that AgNC@MIL-125-NH_2 has a high catalytic activity towards 4-NA hydrogenation, within the same order of magnitude of previously reported works using other Ag functionalized MOFs (AgNC@MIL-101(Fe), *k* = 0.3 min^{-1}).[80]

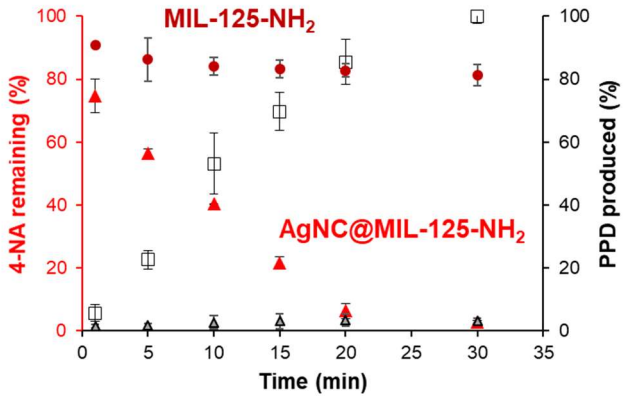

Figure 5. 4-NA (2 mM) hydrogenation kinetics in the presence of AgNC@MIL-125-NH_2 (red triangles, left y axis) and MIL-125-NH_2 (b) (dark red squares, left y axis). The PPD formation in both

experiments was also represented (white squares for AgNC@MIL-125-NH_2, and MIL-125-NH_2 (grey triangles; right y axis).

Conclusions

This work presents an ultrafast two-step photoreduction synthetic protocol for the stabilization of AgNCs within the MIL-125-NH_2 framework, with an average size of 1 nm (~28 Ag atoms) and homogeneously distributed along the MOF crystals. MIL-125-NH_2 framework prevents clusters aggregation and the strong metal-matrix interaction leads to a photoactive composite with a 2.4 eV energy band gap. This synthetic procedure can be in principle applied in other aminated MOFs in a way to achieve small metallic Ag-clusters in their porosity. Further, the AgNC-MOF based photocatalyst here prepared demonstrates great potential for the visible light assisted degradation of challenging emerging organic contaminants in tap water, such as the dye MB and the antibiotic SMT. The photodegradation of contaminants under continuous linear flow using MOFs is performed here for the first time and is among the first reports of MOFs used for continuous wastewater treatment by photodegradation, enabling the purification of 6.50 $L \cdot h^{-1} \cdot g^{-1}$ of SMT contaminated water *via* visible light photocatalytic degradation. Further, considering the results obtained in the 4-NA hydrogenation reaction, AgNC@MIL-125-NH_2 catalysts could be extended to many other industrially important aqueous heterogeneous reactions. By considering the final (real) working conditions (tap water, real contaminants concentration ranges found in natural waters, and continuous flow working conditions which are going to be use on the real scale), and the simultaneous study of potential leaching of the MOF building blocks (normally not considered), this work paves the way for the real future application of MOFs and MOF composites as photocatalysts for the elimination of challenging dyes, antibiotics and other widespread PPCPs in environmental remediation.

Conflicts of interest

There are no conflicts to declare.

Acknowledgements

The work has been supported by IMDEA Energy Foundation, BBVA Foundation (ref: IN[17]_CBB_QUI_0197), Raphuel project (ENE2016-79608-C2-1-R, MINECOAEI/FEDER, UE) and MOFSEIDON project (PID2019-104228RB-I00, MCI/AEI/FEDER, UE). A.A-V. and P.H. want to thank the financial support of Madrid Community (CAM PEJD-2016/IND-2828). S.R. and P.H. acknowledges the financial support of Madrid Community (Recruitment of Young doctors 2017, Talento Modality 2, 2017-T2/IND-5149). P.H. and M.L. acknowledges the Spanish Ramón y Cajal Programme (Grant Agreements 2014-15039 and 2015-18677, respectively). S.R. acknowledges the Spanish Juan de la Cierva Incorporación Fellowship (grant agreement no. IJC2019-038894-I). The authors acknowledge funding from the EU (ERC Consolidator Grant REALNANO 815128 and Grant Agreement nº. 731019 (EUSMI) under the Horizon 2020 Programme). D. A. acknowledges the financial support through the Retos Project from MINECO with reference MAT2017-84385-R for funding.

Notes and references

1 S. Zandaryaa, *A World Sci.*, 2011, **9**, 18–21.
2 I. Ali, M. Asim and T. A. Khan, *J. Environ. Manage.*, 2012, **113**, 170–183.
3 D. J. Lapworth, N. Baran, M. E. Stuart and R. S. Ward, *Environ. Pollut.*, 2012, **163**, 287–303.
4 H. B. Quesada, A. T. A. Baptista, L. F. Cusioli, D. Seibert, C. de Oliveira Bezerra and R. Bergamasco, *Chemosphere*, 2019, **222**, 766–780.
5 A. J. Ebele, M. Abou-Elwafa Abdallah and S. Harrad, *Emerg. Contam.*, 2017, **3**, 1–16.
6 M. Ibáñez, E. Gracia-Lor, L. Bijlsma, E. Morales, L. Pastor and F. Hernández, *J. Hazard. Mater.*, 2013, **260**, 389–398.
7 J. L. Acero, F. J. Benitez, F. J. Real, G. Roldan and E. Rodriguez, *Chem. Eng. J.*, 2013, **219**, 43–50.
8 E. A. Serna-Galvis, A. M. Botero-Coy, D. Martínez-Pachón, A. Moncayo-Lasso, M. Ibáñez, F. Hernández and R. A. Torres-Palma, *Water Res.*, 2019, **154**, 349–360.
9 N. H. Tran, T. Urase, H. H. Ngo, J. Hu and S. L. Ong, *Bioresour. Technol.*, 2013, **146**, 721–731.
10 N. Klamerth, N. Miranda, S. Malato, A. Agüera, A. R. Fernández-Alba, M. I. Maldonado and J. M. Coronado, *Catal. Today*, 2009, **144**, 124–130.
11 S. Wilhelm, A. Henneberg, H. R. Köhler, M. Rault, D. Richter, M. Scheurer, S. Suchail and R. Triebskorn, *Aquat. Toxicol.*, 2017, **192**, 184–197.
12 C. C. Wang, J. R. Li, X. L. Lv, Y. Q. Zhang and G. Guo, *Energy Environ. Sci.*, 2014, **7**, 2831–2867.
13 H. Li, M. Eddaoudi, M. O'Keeffe and O. M. Yaghi, *Nature*, 1999, **402**, 276–279.
14 O. K. Farha, I. Eryazici, N. C. Jeong, B. G. Hauser, C. E. Wilmer, A. A. Sarjeant, R. Q. Snurr, S. T. Nguyen, A. Ö. Yazaydin and J. T. Hupp, *J. Am. Chem. Soc.*, 2012, **134**, 15016–15021.
15 I. M. Hönicke, I. Senkovska, V. Bon, I. A. Baburin, N. Bönisch, S. Raschke, J. D. Evans and S. Kaskel, *Angew. Chemie Int. Ed.*, 2018, **57**, 13780–13783.
16 P. Silva, S. M. F. Vilela, J. P. C. Tomé and F. A. Almeida Paz, *Chem. Soc. Rev.*, 2015, **44**, 6774–6803.
17 U.-H. Lee, A. H. Valekar, Y. K. Hwang and J.-S. Chang, in *The Chemistry of Metal-Organic Frameworks: Synthesis, Characterization, and Applications*, 2016, pp. 551–572.
18 Z. Hasan, J. Jeon and S. H. Jhung, *J. Hazard. Mater.*, 2012, **209**–**210**, 151–157.
19 X. Zhang, J. Wang, X. X. Dong and Y. K. Lv, *Chemosphere*, 2020, **242**, 125144–125159.
20 S. Rojas, J. A. R. Navarro and P. Horcajada, *Dalt. Trans.*, 2021, **50**, 2493–2500.

21 E. Grabowska, A. Zaleska, S. Sorgues, M. Kunst, A. Etcheberry, C. Colbeau-Justin and H. Remita, *J. Phys. Chem. C*, 2013, **117**, 1955–1962.

22 X. Yu, L. Wang and S. M. Cohen, *CrystEngComm*, 2017, **19**, 4126–4136.

23 Y. Liu, Z. Liu, D. Huang, M. Cheng, G. Zeng, C. Lai, C. Zhang, C. Zhou, W. Wang, D. Jiang, H. Wang and B. Shao, *Coord. Chem. Rev.*, 2019, 388, 63–78.

24 X. Liu, R. Dang, W. Dong, X. Huang, J. Tang, H. Gao and G. Wang, *Appl. Catal. B Environ.*, 2017, **209**, 506–513.

25 N. M. Mahmoodi, A. Taghizadeh, M. Taghizadeh and J. Abdi, *J. Hazard. Mater.*, 2019, **378**, 120741.

26 C. P. Joshi, M. S. Bootharaju and O. M. Bakr, *J. Phys. Chem. Lett.*, 2015, 6, 3023–3035.

27 D. A. Islam, A. Chakraborty and H. Acharya, *New J. Chem.*, 2016, **40**, 6745–6751.

28 X. H. Jiang, L. S. Zhang, H. Y. Liu, D. S. Wu, F. Y. Wu, L. Tian, L. L. Liu, J. P. Zou, S. L. Luo and B. B. Chen, *Angew. Chemie - Int. Ed.*, 2020, **59**, 23112–23116.

29 Q. M. Wang, Y. M. Lin and K. G. Liu, *Acc. Chem. Res.*, 2015, **48**, 1570–1579.

30 M. I. Setyawati, X. Yuan, J. Xie and D. T. Leong, *Biomaterials*, 2014, **35**, 6707–6715.

31 T. Soares, D. Ribeiro, C. Proença, R. C. Chisté, E. Fernandes and M. Freitas, *Life Sci.*, 2016, **145**, 247–254.

32 D. A. Islam, A. Chakraborty and H. Acharya, *New J. Chem.*, 2016, **40**, 6745–6751.

33 R. J. T. Houk, B. W. Jacobs, F. El Gabaly, N. N. Chang, A. A. Talin, D. D. Graham, S. D. House, I. M. Robertson and M. D. Allendorf, *Nano Lett.*, 2009, **9**, 3413–3418.

34 F. Su, Q. Jia, Z. Li, M. Wang, L. He, D. Peng, Y. Song, Z. Zhang and S. Fang, *Microporous Mesoporous Mater.*, 2019, **275**, 152–162.

35 B. Han, X. Hu, M. Yu, T. Peng, Y. Li and G. He, *RSC Adv.*, 2018, **8**, 22748–22754.

36 X. Yuan, H. Wang, Y. Wu, G. Zeng, X. Chen, L. Leng, Z. Wu and H. Li, *Appl. Organomet. Chem.*, 2016, **30**, 289–296.

37 AZO, No Title, https://www.azom.com/article.aspx?ArticleID=16650.

38 INSCX, Global Sales of Nanomaterials, https://inscx.com/shop/product/titanium-metal-organic-framework-ti-nh2-mil-125-99-30-40µm/.

39 M. Dan-Hardi, C. Serre, T. Frot, L. Rozes, G. Maurin, C. Sanchez and G. Férey, *J. Am. Chem. Soc.*, 2009, **131**, 10857–10859.

40 A. Arenas-Vivo, G. Amariei, S. Aguado, R. Rosal and P. Horcajada, *Acta Biomater.*, 2019, **97**, 490–500.

41 M. A. Nasalevich, R. Becker, E. V. Ramos-Fernandez, S. Castellanos, S. L. Veber, M. V. Fedin, F. Kapteijn, J. N. H. Reek, J. I. van der Vlugt and J. Gascon, *Energy Environ. Sci.*, 2015, **8**, 364–375.

42 M. De Miguel, F. Ragon, T. Devic, C. Serre, P. Horcajada and H. García, *ChemPhysChem*, 2012, **13**, 3651–3654.

43 N. Askari, M. Beheshti, D. Mowla and M. Farhadian, *Chemosphere*, 2020, **251**, 126453.

44 S. Mosleh and M. R. Rahimi, *Ultrason. Sonochem.*, 2017, **35**, 449–457.

45 Q. Huang, Y. Hu, Y. Pei, J. Zhang and M. Fu, *Appl. Catal. B Environ.*, 2019, **259**, 118106.

46 M. Bahmani, K. Dashtian, D. Mowla, F. Esmaeilzadeh and M. Ghaedi, *J. Hazard. Mater.*, 2020, **393**, 122360.

47 S. Managaki, A. Murata, H. Takada, C. T. Bui and N. H. Chiem, *Environ. Sci. Technol.*, 2007, **41**, 8004–8010.

48 M. Petrovic and P. Verlicchi, *Contrib. to Sci.*, 2014, **10**, 135–150.

49 L. A. Poirier, D. R. Doerge, D. W. Gaylor, M. A. Miller, R. J. Lorentzen, D. A. Casciano, F. F. Kadlubar and B. A. Schweiz, *Regul. Toxicol. Pharmacol.*, 1999, **30**, 217–222.

50 H. Fiege, H.-W. Voges, T. Hamamoto, S. Umemura, T. Iwata, H. Miki, Y. Fujita, H.-J. Buysch, D. Garbe and W. Paulus, *Ullman's Encycl. Ind. Chem.*, 2012, 26, 617–622.

51 M. Zhu, L. Zhang, S. Liu, D. Wang, Y. Qin, Y. Chen, W. Dai, Y. Wang, Q. Xing and J. Zou, *Chinese Chem. Lett.*, 2020, **31**, 1961–1965.

52 L. Maretti, P. S. Billone, Y. Liu and J. C. Scaiano, *J. Am. Chem. Soc.*, 2009, **131**, 13972–13980.

53 N. García-Bosch, M. Liras, I. Quijada-Garrido and O. García, *RSC Adv.*, 2016, **6**, 67643–67650.

54 M. Meilikhov, K. Yusenko, D. Esken, S. Turner, G. Van Tendeloo and R. A. Fischer, *Eur. J. Inorg. Chem.*, 2010, 3701–3714.

55 B. D. Viezbicke, S. Patel, B. E. Davis and D. P. Birnie, *Phys. status solidi*, 2015, **252**, 1700–1710.

56 G. Nibret, S. Ahmad, D. G. Rao, I. Ahmad, M. A. M. U. Shaikh and Z. U. Rehman, *SSRN Electron. J.*, 2019, **26–28**, 1959–1969.

57 L. Collado, A. Reynal, F. Fresno, M. Barawi, C. Escudero, V. Perez-Dieste, J. M. Coronado, D. P. Serrano, J. R. Durrant and V. A. de la Peña O'Shea, *Nat. Commun.*, 2018, **9**, 1–10.

58 S. Nair and B. J. Tatarchuk, *Fuel*, 2010, **89**, 3218–3225.

59 D. Marcinkowski, M. Walesa-Chorab, V. Patroniak, M. Kubicki, G. Kadziolka and B. Michalkiewicz, *New J. Chem.*, 2014, **38**, 604.

60 C. Te Hsieh, W. S. Fan, W. Y. Chen and J. Y. Lin, *Sep. Purif. Technol.*, 2009, **67**, 312–318.

61 A. Gómez-Avilés, V. Muelas-Ramos, J. Bedia, J. J. Rodriguez and C. Belver, *Catalysts*, 2020, **10**, 603.

62 J. Xiao, Q. Shang, Y. Xiong, Q. Zhang, Y. Luo, S. Yu and H. Jiang, *Angew. Chemie*, 2016, **128**, 9535–9539.

63 C. R. Henry, C. Chapon, S. Giorgio and C. Goyhenex, in *Chemisorption and Reactivity on Supported Clusters and Thin Films*, Springer Netherlands, 1997, pp. 117–152.

64 D. J. Lewis, T. M. Day, J. V. MacPherson and Z. Pikramenou, *Chem. Commun.*, 2006, 1433–1435.

65 K. ichi Shimizu, Y. Miyamoto and A. Satsuma, *J. Catal.*, 2010, **270**, 86–94.

66 M. Lamoth, M. Plodinec, L. Scharfenberg, S. Wrabetz, F. Girgsdies, T. Jones, F. Rosowski, R. Horn, R. Schlögl and E. Frei, *ACS Appl. Nano Mater.*, 2019, **2**, 2909–2920.

67 F. Çeçen and O. Aktas, *Activated carbon for water and wastewater treatment: integration of adsorption and biological treatment*, 2011.

68 J. D. S. F. Da Silva, D. L. Malo, G. A. Bataglion, M. N. Eberlin, C. M. Ronconi, S. Alves and G. F. De Sá, *PLoS One*, 2015, **10**,

1–20.
69 S. M. Mirsoleimani-Azizi, P. Setoodeh, F. Samimi, J. Shadmehr, N. Hamedi and M. R. Rahimpour, *J. Environ. Chem. Eng.*, 2018, **6**, 4653–4664.
70 Z. Jia, M. Jiang and G. Wu, *Chem. Eng. J.*, 2017, **307**, 283–290.
71 Z. Ren, J. Luo and Y. Wan, *Chem. Eng. J.*, 2018, **348**, 389–398.
72 H. Wang, S. Zhao, Y. Liu, R. Yao, X. Wang, Y. Cao, D. Ma, M. Zou, A. Cao, X. Feng and B. Wang, *Nat. Commun.*, 2019, 1–9.
73 R. Guo, X. Cai, H. Liu, Z. Yang, Y. Meng, F. Chen, Y. Li and B. Wang, *Environ. Sci. Technol.*, 2019, **53**, 2705–2712.
74 M. Patel, R. Kumar, K. Kishor, T. Mlsna, C. U. Pittman and D. Mohan, *Chem. Rev.*, 2019, **119**, 3510–3673.
75 H. C. Thomas, *J. Am. Chem. Soc.*, 1944, **66**, 1664–1666.
76 H. Li, J. He, K. Chen, Z. Shi, M. Li, P. Guo and L. Wu, *Materials (Basel).*, 2020, **13**, 16–20.
77 J. L. Sotelo, G. Ovejero, A. Rodríguez, S. Álvarez and J. García, *Ind. Eng. Chem. Res.*, 2012, **51**, 5045–5055.
78 P. Dauthal and M. Mukhopadhyay, *Korean J. Chem. Eng.*, 2015, **32**, 837–844.
79 K. Zhang, J. M. Suh, J. W. Choi, H. W. Jang, M. Shokouhimehr and R. S. Varma, *ACS Omega*, 2019, **4**, 483–495.
80 D. A. Islam, A. Chakraborty and H. Acharya, *New J. Chem.*, 2016, **40**, 6745–6751.

